

Dark matter and Higgs boson collider implications of fermions in an abelian-gauged hidden sector

Shrihari Gopalakrishna^a, Seung J. Lee^b, James D. Wells^c

^a *Physics Department, Brookhaven National Laboratory, Upton, NY 11973*

^b *Dept of Particle Physics, Weizmann Institute of Science, Rehovot 76100 Israel*

^c *CERN Theoretical Physics (PH-TH), CH-1211 Geneva 23, Switzerland, and
MCTP, University of Michigan, Ann Arbor, MI 48109*

Abstract

We add fermions to an abelian-gauged hidden sector. We show that the lightest can be the dark matter with the right thermal relic abundance, and discovery is within reach of upcoming dark matter detectors. We also show that these fermions change Higgs boson phenomenology at the Large Hadron Collider (LHC), and in particular could induce a large invisible width to the lightest Higgs boson state. Such an invisibly decaying Higgs boson can be discovered with good significance in the vector boson fusion channel at the LHC.

November 7, 2018

Abelian-Gauged Hidden Sector

We work in the context of the theory motivated and developed in Refs. [1, 2, 3, 4, 5, 6, 7, 8]. We start with the theory in Ref. [7], where the Higgs sector Lagrangian is

$$\begin{aligned} \mathcal{L}_\Phi = & |D_\mu \Phi_{SM}|^2 + |D_\mu \Phi_H|^2 + m_{\Phi_H}^2 |\Phi_H|^2 + m_{\Phi_{SM}}^2 |\Phi_{SM}|^2 \\ & - \lambda |\Phi_{SM}|^4 - \rho |\Phi_H|^4 - \kappa |\Phi_{SM}|^2 |\Phi_H|^2 , \end{aligned} \quad (1)$$

so that $U(1)_X$ is broken spontaneously by $\langle \Phi_H \rangle = \xi/\sqrt{2}$, and electroweak symmetry is broken spontaneously as usual by $\langle \Phi_{SM} \rangle = (0, v/\sqrt{2})^T$. The Higgs sector mixing is defined by two-dimensional rotation equations $\phi_{SM} = c_h h + s_h H$ and $\phi_H = -s_h h + c_h H$, where h, H are the mass eigenstates. We will take the mixing angle s_h to be an input parameter.

If there are new fermions charged under the $U(1)_X$ but are singlets under the SM gauge group, they could impact phenomenology in interesting ways. In particular, the lightest charged fermion is stable and can be the dark matter. Furthermore, the Higgs bosons in the theory are expected to mix and induce Higgs phenomenology significantly different from the SM. Most especially, as we shall show, the Higgs boson will lose significance in all SM channels, and in addition can decay dominantly into the hidden sector fermions and thus be invisibly decaying. Other related works involving Hidden-sector dark matter are discussed in Refs. [9, 10].

Adding Dirac Fermions

We consider a theory with two vector-like pairs (ψ, ψ^c) and (χ, χ^c) that carry $U(1)_X$ charges but not any SM gauge quantum numbers. Since there are no fermions charged under both the SM gauge group and $U(1)_X$, there are no mixed anomalies. The vector-like nature makes the $U(1)_X$ anomaly cancellation trivial. We add the Lagrangian terms (written with Weyl spinors)

$$\begin{aligned} \mathcal{L} \supset & \mathcal{L}_\psi^{CD} + \mathcal{L}_{\psi^c}^{CD} + \mathcal{L}_\chi^{CD} + \mathcal{L}_{\chi^c}^{CD} + \\ & - (\lambda_s \Phi_H \psi \chi + \lambda'_s \Phi_H^* \psi^c \chi^c + h.c.) + \\ & - (M_\psi \psi^c \psi + M_\chi \chi^c \chi + h.c.) , \end{aligned} \quad (2)$$

where the covariant derivative term is

$$\mathcal{L}_\psi^{CD} = \psi^\dagger i \bar{\sigma}^\mu \partial_\mu \psi + g_X \psi^\dagger \bar{\sigma}^\mu q_\psi \psi \hat{X}_\mu , \quad (3)$$

and similarly for the other covariant-derivative terms; q_ψ represents the $U(1)_X$ charge of ψ . We assume that the vector-like masses M_ψ and M_χ are around the electroweak scale. $U(1)_X$ invariance requires $q_{\Phi_H} + q_\psi + q_\chi = 0$. We additionally require $q_{\Phi_H} \neq 0$ since its VEV breaks $U(1)_X$, which then implies that $q_\psi \neq -q_\chi$. Other than these restrictions, the charges can be chosen freely.

There is an accidental Z_2 symmetry under which $\psi, \psi^c, \chi, \chi^c$ are odd, while Φ_H and all SM fields are even. This ensures the stability of the lightest Z_2 odd fermion, which we will identify as the dark-matter candidate.

In addition to the vector-like masses, $U(1)_X$ breaking by $\langle \Phi_H \rangle = \xi/\sqrt{2}$ implies the Dirac masses $m_D \equiv \lambda_s \xi/\sqrt{2}$ and $m'_D \equiv \lambda'_s \xi/\sqrt{2}$. We define the Dirac spinors

$$\Psi \equiv \begin{pmatrix} \psi \\ \psi^c \end{pmatrix} \quad ; \quad \mathcal{X} \equiv \begin{pmatrix} \chi \\ \chi^c \end{pmatrix} , \quad (4)$$

with the charge-conjugate of these spinors given by Ψ^c and \mathcal{X}^c . The mass terms can be written as

$$\mathcal{L}_{\text{mass}} = - (\bar{\Psi}_R \quad \bar{\mathcal{X}}_R^c) \begin{pmatrix} M_\psi & m'_D \\ m_D & M_\chi \end{pmatrix} \begin{pmatrix} \Psi_L \\ \mathcal{X}_L^c \end{pmatrix} + h.c. \quad (5)$$

We go to the mass basis $\{\Psi, \mathcal{X}^c\}_{L,R} \rightarrow \{\Psi_1, \Psi_2\}_{L,R}$ by simple two-dimensional rotations characterized by the angles $\theta_{L,R}$: $\Psi_L = c_{\psi_L} \Psi_{1L} + s_{\psi_L} \Psi_{2L}$, etc., where s_ψ, c_ψ denote the sine and cosine of the angle respectively. There are thus two mass eigenstates, whose masses M_1 and M_2 are straightforwardly computable from the couplings in the lagrangian above.

The Higgs- Ψ - Ψ interactions can be obtained by replacing $m_D \rightarrow m_D(1 + \phi_H/\xi)$ and $m'_D \rightarrow m'_D(1 + \phi_H/\xi)$ in Eq. (5). We find the couplings between the Higgs mass eigenstates (h, H) to the fermion mass eigenstates (Ψ_1, Ψ_2) (Feynman rules)

$$\begin{aligned} \bar{\Psi}_1 \Psi_1 \{h, H\} & : -\frac{i}{\sqrt{2}} \kappa_{11} \{-s_h, c_h\} \\ \bar{\Psi}_2 \Psi_2 \{h, H\} & : -\frac{i}{\sqrt{2}} \kappa_{22} \{-s_h, c_h\} \\ \bar{\Psi}_1 \Psi_2 \{h, H\} & : -\frac{i}{\sqrt{2}} (\kappa_{12} P_L + \kappa_{21} P_R) \{-s_h, c_h\} \\ \bar{\Psi}_2 \Psi_1 \{h, H\} & : -\frac{i}{\sqrt{2}} (\kappa_{21} P_L + \kappa_{12} P_R) \{-s_h, c_h\}, \end{aligned} \quad (6)$$

where we have defined (with all κ assumed real)

$$\begin{aligned} \kappa_{11} & = -\lambda'_s c_{\psi_R} s_{\psi_L} - \lambda_s s_{\psi_R} c_{\psi_L} \\ \kappa_{12} & = \lambda'_s c_{\psi_R} c_{\psi_L} - \lambda_s s_{\psi_R} s_{\psi_L} \\ \kappa_{21} & = -\lambda'_s s_{\psi_R} s_{\psi_L} + \lambda_s c_{\psi_R} c_{\psi_L} \\ \kappa_{22} & = \lambda'_s s_{\psi_R} c_{\psi_L} + \lambda_s c_{\psi_R} s_{\psi_L} \end{aligned} \quad (7)$$

An alternative theory could be presented with just one vector-like pair of fermions. Using Weyl spinors we can write $\mathcal{L} = -\lambda_m \Phi_H \psi \psi - \lambda'_m \Phi_H^* \psi^c \psi^c - M_\psi \psi \psi^c + h.c.$ This requires the $U(1)_X$ charge assignment $q_H = -2q_\psi$ and, of course, $q_{\psi^c} = -q_\psi$. We define a 4-component spinor $\Psi \equiv (\psi \ \psi^c)$ with its complex conjugate Ψ^c , and after $U(1)_X$ breaking we can diagonalize the mass matrix and write the theory in terms of two 4-component mass eigenstate Majorana spinors Ψ_1^M and Ψ_2^M given as linear combinations of Ψ and Ψ^c . The theory so obtained after $U(1)_X$ breaking is $\mathcal{L} \supset \frac{1}{2} \bar{\Psi}_i^M (\not{\partial} - M_{\psi_i}) \Psi_i^M - \frac{1}{2} \kappa_{ij}^M \phi_H \bar{\Psi}_i^M \Psi_j^M$ (with $i, j = \{1, 2\}$) where the extra factor of 1/2 is included as usual in defining κ^M for a Majorana fermion in order to cancel the factor of two from the two Wick contractions for a Majorana fermion that arises when computing a matrix element. The $\bar{\Psi}^M \Psi^M \{h, H\}$ Feynman rules

are as given in Eq. (6) with the κ^M definition similar to Eq. (7) except for the inclusion of a factor of 1/2 in the left-hand-side for the above reason. The phenomenology of this theory is qualitatively similar to the Dirac theory discussed above. Although our subsequent discussion will mainly be focused on the two Dirac fermions case described above, we will comment later on what things change for the Majorana case.

To complete the description of our Feynman rules conventions we provide the triple Higgs boson interaction vertices. Our Lagrangian provides, after $U(1)_X$ and electroweak symmetry breaking, $\mathcal{L} \supset -\frac{\kappa\xi}{2}\phi_{SM}^2\phi_H - \frac{\kappa v}{2}\phi_{SM}\phi_H^2 - \lambda v\phi_{SM}^3 - \rho\xi\phi_H^3$ which in the mass basis implies the following relevant Feynman rules:

$$hhh : -\frac{i}{\sqrt{2}}vc_h\kappa_{3\phi} , \quad Hhh : -\frac{i}{\sqrt{2}}\xi s_h\kappa_{H2h} , \quad (8)$$

These serve to define the dimensionless cubic couplings $\kappa_{3\phi}$ and κ_{H2h} , and while we can show these in terms of the fundamental Lagrangian parameters, it is sufficient for our purposes to treat them as effective input parameters.

Parameters of the Theory

We will explore the cosmological, direct-detection and collider implications of the theory we have outlined. We will restrict ourselves to the lightest (and therefore stable) hidden sector fermion Ψ_1 (denoted as ψ henceforth), although many interesting effects can occur due to transitions to and from more massive states such as the Ψ_2 . We will take an effective theory approach and note that the phenomenology is identical to a large class of theories with a hidden sector fermion ψ interacting via the Higgs in the way we have outlined. The relevant parameters are: M_ψ , κ_{11} , $\kappa_{3\phi}$, s_h and m_h .

Partial-wave unitarity imposes upper limits on combinations of the parameters κ_{11} , s_h , $\kappa_{3\phi}$. For instance, the total cross-section $\sigma(\psi\psi \rightarrow YY)$, where YY generically denotes a pair of final state particles, is bounded by unitarity [11] as $\sigma_\ell < 16\pi(2\ell + 1)/s$, where σ_ℓ denotes the cross-section in the ℓ^{th} partial-wave, and s is the usual Mandelstam variable. To correctly obtain the bound one needs to impose the bound on the partial waves, but we present below a sufficient condition using the total cross-section to show that the parameter ranges we will consider in this work are safe with respect to unitarity constraints. For non-relativistic ψ , assuming that the unitarity bound is saturated by $\sigma(\psi\psi \rightarrow \psi\psi)$ we find the bound $\kappa_{11}s_h \lesssim 2.5$, with the other final-states giving weaker bounds for $M_\psi < 160$ GeV. For $M_\psi > 160$ GeV, $\sigma(\psi\psi \rightarrow W^+W^-)$ gives the strongest bound $\kappa_{11}s_h c_h \lesssim 1$. Also, when kinematically allowed, $\sigma(\psi\psi \rightarrow hh)$ gives an additional constraint that is rather weak $\kappa_{11}\kappa_{3\phi}s_h c_h \lesssim 10^4$. We further note that the behavior of the cross-sections is such that the bound only gets weaker as the CM energy becomes large compared to M_ψ and m_h .

Relic density

$\psi\psi$ annihilations into the W^+W^- , ZZ , hh , $t\bar{t}$ final states will be important if they are kinematically accessible, and if not, the dominant channel is into $b\bar{b}$. We compute the annihilation cross-section in the mass basis including s , t and u -channel graphs.

The ψ are non-relativistic during freeze-out and the annihilation cross-sections can be written in the non-relativistic limit [12] to leading order in $|\mathbf{p}_\psi|$, the 3-momentum magnitude of the incoming ψ , with $|\mathbf{p}_\psi|^2/M_\psi^2 = v_{rel}^2/4 + O(v_{rel}^4)$, $s = s_0(1 + v_{rel}^2/4) + O(v_{rel}^4)$, where $s_0 \equiv 4M_\psi^2$, and v_{rel} is the relative velocity between the colliding ψ . We can write $\sigma v_{rel} = a + b v_{rel}^2 + O(v_{rel}^4)$, defining a and b as used commonly in the literature. The thermally averaged cross-section is then given by [13]: $\langle\sigma v\rangle(x_f) \approx a + (6b - 9a)/x_f$ during freeze-out, where $x_f \equiv M_\psi/T_f$ is the unitless measure of the freeze-out temperature T_f .

Once the thermally averaged cross-section $\langle\sigma v\rangle$ is obtained, we can compute the ratio of the present relic density to the critical energy density (for summaries, see for example Refs. [14, 15, 16]), which is given by

$$\Omega_0 h^2 = x_f \frac{10^{-29} \text{ eV}^{-2}}{\langle\sigma v\rangle(x_f)}, \quad (9)$$

where $h^2 \approx 0.5$, and we can take $x_f \approx 25$ to a good approximation since it depends only mildly (logarithmically) on the parameters. To obtain the observed dark matter relic density we need $\langle\sigma v\rangle \sim 1.5 \times 10^{-9} \text{ GeV}^{-2}$.

Next, we present analytical formulas for the self-annihilation cross-section into the dominant channels. In the annihilation cross-sections below, we will omit showing the decay widths of the particles in the propagators, and also not show the heavy Higgs contribution since we take $m_H \gg M_\psi$, although we will include it in the numerical analysis to be presented.

In the center-of-mass (CM) frame, the annihilation cross-section of a pair of Dirac ψ into SM $f\bar{f}$ is given by

$$\sigma(\psi\bar{\psi} \rightarrow f\bar{f}) \approx \frac{N_c \kappa_{11}^2 \lambda_f^2 s_h^2 c_h^2}{8\pi v_{rel}} \frac{|\mathbf{p}_\psi|^2}{(s - m_h^2)^2} \left(1 - \frac{4m_f^2}{s}\right)^{3/2}, \quad (10)$$

where $N_c = 3$ for a fermion in the fundamental of $SU(3)_c$, and $\lambda_f/\sqrt{2}$ is the $\phi_{SM} f \bar{f}$ Yukawa coupling. Eq. (10) is valid for both $b\bar{b}$ and $t\bar{t}$ final states. For $M_\psi > m_W$, the W^+W^- channel is accessible, and its cross-section is given by

$$\sigma(\psi\bar{\psi} \rightarrow W^+W^-) \approx \frac{\kappa_{11}^2 g^4 s_h^2 c_h^2 v_{EW}^2}{8\pi v_{rel}} \frac{|\mathbf{p}_\psi|^2}{(s - m_h^2)^2} \sqrt{1 - \frac{4m_W^2}{s}} \left[\frac{1}{2} + \frac{(s/2 - m_W^2)^2}{4m_W^4} \right], \quad (11)$$

where $v_{EW} = 246 \text{ GeV}$. For $M_\psi > m_Z$, the ZZ final state will be accessible also, and the annihilation cross-section is similar to Eq. (11) but with an extra factor of $1/2c_W^4$, and with $m_W \rightarrow m_Z$. For $M_\psi > m_h$ the hh final state will be open, and including the s , t and u -channel graphs, we find the cross-section

$$\begin{aligned} \sigma(\psi\bar{\psi} \rightarrow hh) \approx & \frac{\kappa_{11}^2 s_h^2 |\mathbf{p}_\psi|^2}{8\pi v_{rel} M_\psi^2} \sqrt{1 - \frac{4m_h^2}{s}} \left\{ \frac{\kappa_{3\phi}^2 c_h^2 v_{EW}^2}{16 (s - m_h^2)^2} - \frac{\kappa_{3\phi} \kappa_{11} c_h s_h v_{EW} M_\psi}{2 (s - m_h^2) (t_0 - M_\psi^2)} \right. \\ & \cdot \left[1 - \frac{t_0}{3 (t_0 - M_\psi^2)} \right] + \frac{\kappa_{11}^2 s_h^2 M_\psi^2}{(t_0 - M_\psi^2)^2} \left[1 - \frac{t_0}{12 (t_0 - M_\psi^2)} \right] \left. \right\} \quad (12) \end{aligned}$$

with the dimensionless Higgs cubic coupling $\kappa_{3\phi}$ as given in Eq. (8). We have defined $t_0 \equiv -|\mathbf{k}_h|^2$ to be the Mandelstam variable t in the $\mathbf{p}_\psi \rightarrow 0$ limit with \mathbf{k}_h being the three momentum of the outgoing Higgs boson.

The reason that all cross-sections above are proportional to $|\mathbf{p}_\psi|$ follows from the CP transformation property of the initial, intermediate and final states, and angular-momentum conservation. Under a CP transformation, the two-fermion initial state transforms as $(-1)^{L+S} \times (-1)^{L+1} = (-1)^{S+1}$, shown split up into the C and P transformation factors respectively, where L is the total orbital angular momentum and S the total spin. For the s -channel graphs involving the intermediate CP -even scalar Higgs boson h , the above CP transformation property and angular momentum conservation imply that the initial state has to be in $L = 1$ (p -wave) and $S = 1$ configuration. For the t -channel graph into the hh final state the CP transformation property, angular momentum conservation and the requirement that the two-boson final state be symmetric under interchange implies that the two-fermion initial state has to again be in the $L = 1$ (p -wave) and $S = 1$ configuration. In either case, since the 2-fermion initial state has to be in a p -wave configuration the matrix-element goes to zero as $|\mathbf{p}_\psi| \rightarrow 0$. Therefore, the coefficient a is zero since there is no velocity independent piece in the annihilation cross-section.

We show in Fig. 1 the (0.1, 0.2, 0.3) contours of Ω_{dm0} in the M_ψ - κ_{11} and m_h - s_h planes, with the parameters not varied in the plots fixed at $M_\psi = 200$ GeV, $m_h = 120$ GeV, $s_h = 0.25$, $\kappa_{11} = 2.0$, $\kappa_{3\phi} = 1$, $m_H = 1$ TeV, $\kappa_{H2h} = 1$ and $\xi = 1$ TeV. This benchmark point results in $\Omega_{dm} \approx 0.2$. The present experimental data on the dark matter relic density is $\Omega_{dm} = 0.222 \pm 0.02$, inferred from the following data [11]: total matter density $\Omega_m h^2 = 0.132 \pm 0.004$, baryonic matter density $\Omega_b h^2 = 0.0219 \pm 0.0007$, and $h = 0.704 \pm 0.016$. We see that there exists regions of parameter space that are consistent with the present experimental observations. The region $\Omega_0 < 0.2$ is still allowed but without the ψ being all of the dark matter, while the region $\Omega_0 > 0.3$ is excluded since the ψ would overclose the universe. The contours funnel-down at $M_\psi \simeq 500$ GeV due to a resonant annihilation through the heavy Higgs boson, which is taken here to be 1 TeV. In the region $m_h > 2M_\psi$, the $h \rightarrow \psi\psi$ decay is allowed, implying an invisibly decaying Higgs at a collider. This connection will be explored in a later section.

The Majorana case is qualitatively similar to the Dirac case above. In relating to the number density of the dark matter relic, there is only one species for the Majorana case (rather than two, particle and anti-particle, for the Dirac case), implying a relative factor of 1/2 in the $\langle\sigma v\rangle$ for the Majorana case. (As we have already noted, the coupling for the Majorana case is defined with a relative factor of 1/2 to cancel the factor of two from the two Wick contractions.) The exact values of the Lagrangian parameters that will result in the correct relic density will therefore be different, but will result in qualitatively similar plots. We will therefore not repeat the plots for this case.

Direct Detection of Dark Matter

Many experiments are underway currently to directly detect dark matter, and still more are proposed to improve the sensitivity. In order to ascertain the prospects of directly observing ψ in the $U(1)_X$ framework we are considering, we compute the elastic ψ -nucleon

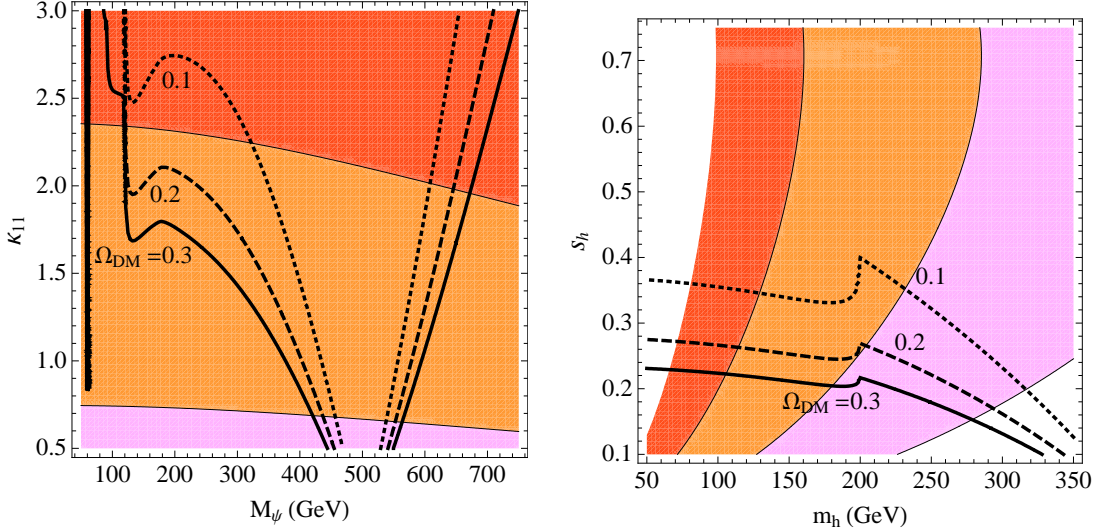


Figure 1: Contours of $\Omega_{dm0} = 0.1, 0.2, 0.3$ (dot, dash, solid) in the M_ψ - κ_{11} and m_h - s_h planes. The parameters not varied in the plots are fixed at $M_\psi = 200$ GeV, $m_h = 120$ GeV, $s_h = 0.25$, $\kappa_{11} = 2$, $\kappa_{3\phi} = 1$, $m_H = 1$ TeV, $\kappa_{H2h} = 1$ and $\xi = 1$ TeV. The direct-detection $\psi - N$ cross-section are shown as shaded regions: $\sigma \gtrsim 10^{-43}$ cm² (dark-shade) is already excluded by experiments. $\sigma \gtrsim 10^{-44}$ cm² (medium-shade), and $\sigma \gtrsim 10^{-45}$ cm² (light-shade), the latter two will be probed in upcoming experiments.

cross-section due to the t -channel exchange of the Higgs boson. The typical dark-matter velocity in our galaxy is about 270 km/s [14], which implies $v_\psi \sim 10^{-3}$, and the ψ is quite non-relativistic. In the CM frame, in the non-relativistic limit, we find the elastic cross-section

$$\sigma(\psi N \rightarrow \psi N) \approx \frac{\kappa_{11}^2 s_h^2 c_h^2 \lambda_N^2 (|\mathbf{p}_\psi|^2 + m_N^2)}{8\pi v_{rel} m_h^4}, \quad (13)$$

where $|\mathbf{p}_\psi| \approx M_\psi v_\psi$, $m_N \approx 1$ GeV is the nucleon mass, $\lambda_N/\sqrt{2}$ is the effective $h\bar{N}N$ coupling, and we have ignored the Mandelstam variable t in comparison to m_h^2 in the Higgs propagator which give a contribution of order $|\mathbf{p}_\psi|^2 m_N^2/m_h^2$. We take $\lambda_N \approx 2 \times 10^{-3}$ [17, 14] which includes the Higgs tree-level coupling to light quarks (u, d, s), and the heavy-quark-loop two-gluon couplings.

To illustrate, for $\kappa_{11} = 2.0$, $s_h = 0.25$, $M_\psi = 200$ GeV, $m_h = 120$ GeV, we find $\sigma \approx 1.9 \times 10^{-16}$ GeV⁻² = 7×10^{-44} cm². This is very interesting as the presently ongoing experiments [18] are probing this range of cross-sections. With all other parameters fixed as above, as m_h is increased to 350 GeV, the direct-detection cross-section falls smoothly to about 10^{-45} cm². In Fig. 1 we show the direct detection cross-section as shaded regions; from the compilation in Ref. [18], the dark-shaded region ($\sigma \gtrsim 10^{-43}$ cm²) is excluded by present bounds from direct detection searches [19, 20], while the medium-shaded ($\sigma \gtrsim 10^{-44}$ cm²) and the light-shaded ($\sigma \gtrsim 10^{-45}$ cm²) regions will be probed by upcoming experiments, such as Super-CDMS and Xenon 1-ton [21]. We have defined our model into the package MicrOMEGAs [22] and checked that our analytical results agree with the full numerical

treatment reasonably well.

Higgs Boson Decays

In addition to the usual SM decay modes, if $M_\psi < m_h/2$, the decay $h \rightarrow \psi\bar{\psi}$ is kinematically allowed, leading to an invisible decay mode for the Higgs boson. Here, we explore how the Higgs decay is affected if this is the case. One should note that if kinematically allowed, the Higgs can decay into a pair of $U(1)_X$ gauge fields (X_μ), which was the subject of Ref. [7]. We will not include the $h \rightarrow XX$ decay mode explicitly in our analysis here, but in regions of parameter space where this is present, its effect would be to decrease all branching ratios discussed in this work. For simplicity, we will consider only on-shell 2-body decays and do not include virtual 3-body modes. Also, we will use the narrow-width approximation in all decay chains.

The Higgs decay width is easily computed using the coupling in Eq. (6). For a Dirac ψ , the invisible decay width of the Higgs boson is given by

$$\Gamma(h \rightarrow \psi\bar{\psi}) = \frac{\kappa_{11}^2 s_h^2}{16\pi} m_h \left(1 - \frac{4M_\psi^2}{m_h^2}\right)^{3/2}. \quad (14)$$

The partial decay width to a SM fermion pair $f\bar{f}$ is given by

$$\Gamma(h \rightarrow f\bar{f}) = \frac{N_c g^2 m_f^2 c_h^2}{32\pi m_W^2} m_h \left(1 - \frac{4m_f^2}{m_h^2}\right), \quad (15)$$

where $N_c = 3$ is for a fermion in the fundamental of $SU(3)_c$. The Higgs partial width to a SM gauge boson pair is given by

$$\Gamma(h \rightarrow W^+W^-) = \frac{g^2 c_h^2}{64\pi m_W^2} m_h^3 \sqrt{1 - \frac{4m_W^2}{m_h^2}} \left(1 - \frac{4m_W^2}{m_h^2} + \frac{12m_W^4}{m_h^4}\right), \quad (16)$$

$$\Gamma(h \rightarrow ZZ) = \frac{g^2 c_h^2}{128\pi m_W^2} m_h^3 \sqrt{1 - \frac{4m_Z^2}{m_h^2}} \left(1 - \frac{4m_Z^2}{m_h^2} + \frac{12m_Z^4}{m_h^4}\right). \quad (17)$$

As mentioned, the $h \rightarrow \psi\psi$ offers a new decay mode in the $U(1)_X$ model, and in Fig. 2 (left) we show the Higgs BR, and a comparison to a few SM modes (right), with the other parameters fixed at $M_\psi = 58.5$ GeV, $s_h = 0.25$, $\kappa_{11} = 2.0$, $\kappa_{3\phi} = 1.0$ and $m_H = 1$ TeV. These parameter values result in the correct relic-density for $m_h = 120$ GeV. In this light Higgs and small M_ψ region where the $b\bar{b}$ channel is the dominant final-state, an acceptable relic-density is obtained only when $m_h \approx 2M_\psi$, i.e. when the Higgs boson pole enhances the cross-section which otherwise is generically too small due to the small b Yukawa coupling. Thus, for the m_h range shown in the figure and for the parameter values shown above, the correct relic-density is obtained only for $m_h \approx 120$ GeV.

For a relatively light Higgs boson ($m_h < 2m_W$) and with $M_\psi \lesssim m_h/2$ the invisible BR dominates in the $U(1)_X$ scenario. For $M_\psi \lesssim 60$ GeV, we find $\Gamma_h(m_h = 120 \text{ GeV}) \approx 5 \times 10^{-3}$ GeV and $\Gamma_h(m_h = 200 \text{ GeV}) \approx 2$ GeV. For smallish s_h , the invisible BR is not as

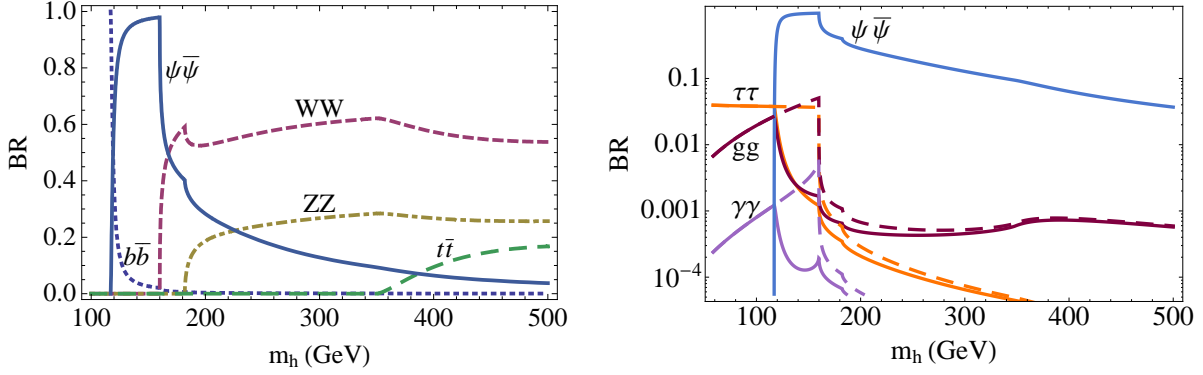


Figure 2: The left plot shows the Higgs BR into invisible, bb , WW , ZZ and tt (thick-solid, dotted, dashed, dash-dot and thin), as a function of the Higgs mass, and in the right plot, the solid curves show the light Higgs BR in the $U(1)_X$ model, with the dashed curves showing the SM Higgs BR's. The other parameters are fixed at $M_\psi = 58.5$ GeV, $s_h = 0.25$, $\kappa_{11} = 2.0$, $\kappa_{3\phi} = 1.0$ and $m_H = 1$ TeV.

large for a heavier Higgs boson since the SM Higgs boson already has a sizable width due to $h \rightarrow W^+W^-$, etc. When the invisible BR is large, as we will show in greater detail in the following, the SM BRs, for example, into $b\bar{b}$ and the $\tau^+\tau^-$ are suppressed, implying that the standard search channels at the LHC will have a reduced significance. We will however show that the invisible mode holds promise for the discovery of the Higgs in this scenario.

The parts of the parameter space that yield the correct dark matter relic density have been discussed earlier (see Fig. 1). We impose the requirement that the relic density should be in the experimentally measured range by scanning over $M_\psi \sim 60$ GeV, and show in Fig. 3 the corresponding BR_{inv} as a function of κ_{11} (see Eq. (6)), with $\kappa_{3\phi} = 1.0$ and $m_H = 1$ TeV held fixed. We see that a significant BR_{inv} is possible while giving the required Ω_0 and being consistent with present direct-detection limits, with the general trend of increasing BR_{inv} for increasing κ_{11} or s_h . Here we have shown only the points that satisfy the direct-detection cross-section $\sigma < 10^{-43}$ cm², to be consistent with current experimental results [18]. For a larger Higgs mass we find qualitatively similar invisible BR with larger values of κ_{11} preferred.

For the Majorana case, since the two final state particles are identical, the phase-space integration results in a factor of 1/2 compared to the Dirac case. Therefore the decay rate for the Majorana case is 1/2 of the Dirac case. As we have already commented, note that the coupling in the Majorana case is defined with a factor of 1/2 compared to the Dirac case. Again, we will not repeat the plots for the Majorana case since they are qualitatively similar to the Dirac case presented previously.

LHC Higgs Boson Phenomenology

In order to see how the suppression of the SM modes will affect the significance in the standard search channels, we estimate the ratio of the discovery significance of the light Higgs in the $gg \rightarrow h \rightarrow \gamma\gamma$, $gg \rightarrow h \rightarrow ZZ \rightarrow 4\ell$ and $gg \rightarrow h \rightarrow WW \rightarrow 2\ell 2\nu$ channels to those of a SM Higgs boson with the same mass. An approximate formula for the ratio of the

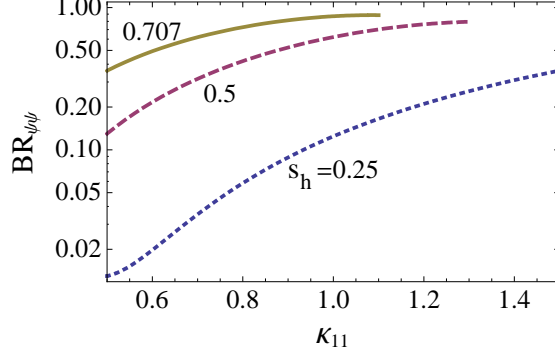


Figure 3: The BR_{inv} as a function of κ_{11} for $m_h = 120$ GeV for $s_h = 0.25, 0.5, 0.707$ (dotted, dashed, solid) with M_ψ adjusted to give the correct dark matter relic density (Ω_0). The other parameters are fixed at $\kappa_{3\phi} = 1.0$ and $m_H = 1$ TeV.

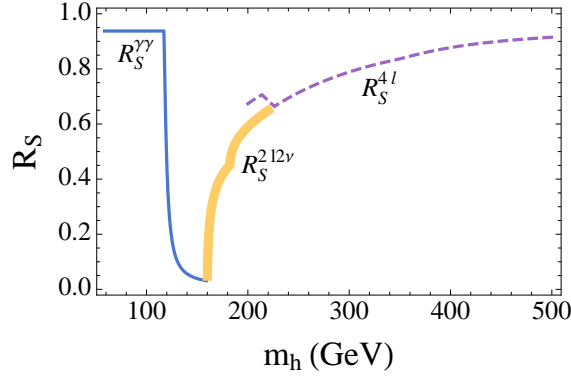


Figure 4: The ratio of the LHC Higgs discovery significance in the $U(1)_X$ model to that in the SM for $M_\psi = 58.5$ GeV, $\kappa_{11} = 2.0$, $s_h = 0.25$, $\kappa_{3\phi} = 1$ and $m_H = 1$ TeV, in the $h \rightarrow \gamma\gamma$, $h \rightarrow ZZ \rightarrow 4\ell$ and $h \rightarrow WW \rightarrow 2\ell 2\nu$ channels.

Higgs discovery significance in the $U(1)_X$ model compared to that in the SM for the same mass in the $gg \rightarrow h \rightarrow XX$ channel can be defined as

$$R_S^{XX} \equiv \frac{S(h)}{S(h_{SM})} = \frac{\Gamma(h \rightarrow gg) B(h \rightarrow XX)}{\Gamma(h_{SM} \rightarrow gg) B(h_{SM} \rightarrow XX)} \cdot F_{XX}(\Gamma) \quad (18)$$

where

$$F_{XX}(\Gamma) = \sqrt{\frac{\max(\Gamma_{\text{tot}}(h_{SM}), \Delta M_{XX})}{\max(\Gamma_{\text{tot}}(h), \Delta M_{XX})}}, \quad (19)$$

if the final state is a resonance (i.e., $\gamma\gamma$ or 4ℓ) and $F_{XX}(\Gamma) = 1$ otherwise. Although as the Higgs boson width gets smaller the signal to background ratio increases, the finite detector resolution of the invariant mass (ΔM_{XX}) limits this, which is accounted for by F_{XX} .

Fig. 4 shows $R_S^{\gamma\gamma, 4\ell, 2\ell 2\nu}$. The $h \rightarrow \gamma\gamma$ channel is the primary discovery channel for $m_h \lesssim 150$ GeV in the SM, and we see that when the invisible Higgs BR is large, the

Table 1: The $pp \rightarrow jjh \rightarrow jj\cancel{E}_T$ channel vector boson fusion signal and background cross-sections from Ref. [23], and the luminosity required for 5σ significance. These are after the cuts shown in Eq. (20).

m_h (GeV)	σ_S (fb)	σ_B (fb)	$\mathcal{L}_{5\sigma}$ (fb^{-1})
120	$97 \cdot c_h^2 BR_{inv}$	167	$0.44 / (BR_{inv}^2 c_h^4)$
200	$77 \cdot c_h^2 BR_{inv}$	167	$0.7 / (BR_{inv}^2 c_h^4)$
300	$56 \cdot c_h^2 BR_{inv}$	167	$1.3 / (BR_{inv}^2 c_h^4)$

significance in this channel in the $U(1)_X$ model deteriorates as anticipated. In the SM, the 4ℓ channel is the most important discovery channel for $m_h \gtrsim 200$ GeV, and we find from $R_S^{4\ell}$ in our model that for $s_h = 0.25$ this channel is still viable, but for larger mixing angle, $s_h = 0.5$, that it is not until $m_h \approx 350$ GeV. From $R_S^{2l2\nu}$ we see that for the Higgs mass between 160 – 200 GeV the $h \rightarrow WW \rightarrow 2l2\nu$ channel, which is the most important channel in the SM, loses its efficiency. Since the Higgs decay channels into SM modes diminish in significance, we turn next to the prospects of a new channel – the invisible decay mode – as a means of discovering the Higgs.

Invisible Decays of the Higgs Boson

To detect an invisibly decaying Higgs boson, we have to look at associated production in order to trigger on the event. Here we consider the jjh channel (vector boson fusion) [23, 24], and Zh associated production [25, 26, 27, 28]. The $t\bar{t}h$ channel [29] is also a possibility but we will not discuss this here. An invisibly decaying Higgs has also been discussed in other contexts in Refs. [30, 31].

jjh channel: The Higgs boson can be produced via vector boson fusion at the LHC, followed by the invisible decay of the Higgs boson. The signature for this mode is two forward tagging jets plus missing energy, i.e., $j j + \cancel{E}_T$. This channel has been analyzed in Ref. [23], which we use to obtain significances in the $U(1)_X$ model by multiplying the signal cross-section given there by $BR_{inv} c_h^2$. The backgrounds included there are QCD and EW Zjj and Wjj . In Table 1 we show the signal (σ_S) and background (σ_B) cross-sections, after the cuts

$$\begin{aligned}
 p_T^j &> 40, \quad |\eta_j| < 5.0, \quad |\eta_{j_1} - \eta_{j_2}| > 4.4, \quad \eta_{j_1} \cdot \eta_{j_2} < 0, \\
 \cancel{p}_T &> 100 \text{ GeV}, \quad M_{jj} > 1200 \text{ GeV}, \quad \phi_{jj} < 1.
 \end{aligned}
 \tag{20}$$

The luminosity required for 5σ statistical significance ($\mathcal{L}_{5\sigma}$) in the $U(1)_X$ model scales as $1/(BR_{inv}^2 c_h^4)$ which we have factored out in the last column. For example, for $m_h = 120$ GeV, $BR_{inv} = 0.75$ and $s_h = 0.5$, we would require a luminosity of 1.4 fb^{-1} for 5σ statistical significance. Alternatively, with 10 fb^{-1} , we can probe BR_{inv} down to about 26% at 5σ . We thus see that in this channel, the prospect of discovering an invisibly decaying Higgs boson in the $U(1)_X$ scenario is excellent. The significance remains quite good even for heavier Higgs masses as can be seen from Table 1. Detailed experimental analyses that take into account additional QCD backgrounds and detector effects are being analyzed [32].

Table 2: The $pp \rightarrow Zh \rightarrow \ell^+\ell^- \cancel{E}_T$ channel signal and background cross-sections and the luminosity required for 5σ significance. The background cross-section is from Ref. [25]. These are after the cuts shown in Eq. (21).

m_h (GeV)	σ_S (fb)	σ_B (fb)	$\mathcal{L}_{5\sigma}$ (fb^{-1})
120	$9 \cdot c_h^2 BR_{inv}$	26.3	$8 / (BR_{inv}^2 c_h^4)$
200	$3.4 \cdot c_h^2 BR_{inv}$	26.3	$58 / (BR_{inv}^2 c_h^4)$
300	$1.1 \cdot c_h^2 BR_{inv}$	26.3	$543 / (BR_{inv}^2 c_h^4)$

Zh channel: In the Zh channel, we focus on the leptonic decay mode of the Z , giving the signature $\ell^+\ell^- + \cancel{E}_T$. This has been analyzed in Ref. [25] for the $m_h = 120, 140, 160$ GeV cases using the cuts

$$p_{T\ell} > 10, |\eta_\ell| < 2.5, \cancel{p}_T > 100 \text{ GeV}, |M_{\ell^+\ell^-} - m_Z| < 10 \text{ GeV}. \quad (21)$$

We adopt the same cuts given in Eq. (21) and compute the signal cross-section using the Monte Carlo package CalcHEP [33]. We use the ZZ , WW , ZW , and $Z + j$ background cross-sections given in Ref. [25], where it is pointed out that with the large $\cancel{p}_T > 100$ GeV cut, the $Z + j$ background [34] is adequately small. We show the signal (σ_S) and background (σ_B) cross-sections after cuts in Table 2. We have checked that our signal cross-section for $m_h = 120$ GeV agrees with that in Ref. [25]. From Table 2, we see for example, for $m_h = 120$ GeV, $BR_{inv} = 0.75$ and $s_h = 0.5$, we would require a luminosity of 25 fb^{-1} for 5σ statistical significance. Alternatively, with 100 fb^{-1} , we can probe BR_{inv} down to about 38% at 5σ . As Table 2 shows, the luminosity required becomes rather large for heavier Higgs masses.

In conclusion, we have shown that fermions in an abelian-gauged hidden sector can be the dark-matter observed cosmologically since they are stable due to an accidental Z_2 symmetry, and the experimentally observed relic-density is obtained for natural values of the Lagrangian parameters. The prospects for directly detecting these fermions in upcoming experiments are excellent. We showed that these fermions can potentially be discovered at the LHC by looking for invisibly decaying Higgs bosons in the vector boson fusion channel.

Acknowledgments: We thank S. Dawson, B. Kilgore, F. Paige, A. Rajaraman, C. Sturm, T. Tait and C. Wagner for valuable discussions. We also thank A. Pukhov for help with micrOMEGAs. SG is supported in part by the DOE grant DE-AC02-98CH10886 (BNL). We thank KITP, Santa Barbara, for hospitality during the ‘‘Physics of the LHC’’ workshop where part of this work was carried out.

References

- [1] R. Schabinger and J. D. Wells, Phys. Rev. D **72**, 093007 (2005) [arXiv:hep-ph/0509209].
- [2] M. J. Strassler and K. M. Zurek, Phys. Lett. B **651**, 374 (2007) [arXiv:hep-ph/0604261].

- [3] J. Kumar and J. D. Wells, Phys. Rev. D **74**, 115017 (2006) [arXiv:hep-ph/0606183].
- [4] M. Bowen, Y. Cui and J. D. Wells, JHEP **0703**, 036 (2007) [arXiv:hep-ph/0701035].
- [5] W. F. Chang, J. N. Ng and J. M. S. Wu, Phys. Rev. D **75**, 115016 (2007) [arXiv:hep-ph/0701254].
- [6] J. March-Russell, S. M. West, D. Cumberbatch and D. Hooper, JHEP **0807**, 058 (2008) [arXiv:0801.3440 [hep-ph]].
- [7] S. Gopalakrishna, S. Jung and J. D. Wells, Phys. Rev. D **78**, 055002 (2008) [arXiv:0801.3456 [hep-ph]].
- [8] J. L. Feng, H. Tu and H. B. Yu, JCAP **0810**, 043 (2008) [arXiv:0808.2318 [hep-ph]].
- [9] Y. G. Kim, K. Y. Lee and S. Shin, JHEP **0805**, 100 (2008) [arXiv:0803.2932 [hep-ph]].
- [10] D. Feldman, Z. Liu and P. Nath, Phys. Rev. D **75**, 115001 (2007) [arXiv:hep-ph/0702123].
- [11] W. M. Yao *et al.* [Particle Data Group], J. Phys. G **33**, 1 (2006) and 2007 partial update for the 2008 edition available on the PDG WWW pages (URL: <http://pdg.lbl.gov/>).
- [12] J. D. Wells, arXiv:hep-ph/9404219.
- [13] M. Srednicki, R. Watkins and K. A. Olive, Nucl. Phys. B **310**, 693 (1988). P. Gondolo and G. Gelmini, Nucl. Phys. B **360**, 145 (1991).
- [14] G. Bertone, D. Hooper and J. Silk, Phys. Rept. **405**, 279 (2005) [arXiv:hep-ph/0404175].
- [15] G. Servant and T. M. P. Tait, Nucl. Phys. B **650**, 391 (2003) [arXiv:hep-ph/0206071].
- [16] S. Gopalakrishna, A. de Gouvea and W. Porod, JCAP **0605**, 005 (2006) [arXiv:hep-ph/0602027].
- [17] M. A. Shifman, A. I. Vainshtein and V. I. Zakharov, Phys. Lett. B **78**, 443 (1978).
- [18] Rick Gaitskell, Vuk Mandic and Jeff Filippini, <http://dmtools.berkeley.edu/limitplots/>.
- [19] Z. Ahmed *et al.* [CDMS Collaboration], Phys. Rev. Lett. **102** (2009) 011301 [arXiv:0802.3530].
- [20] J. Angle *et al.* [XENON Collaboration], Phys. Rev. Lett. **100** (2008) 021303 [arXiv:0706.0039].
- [21] For the Xenon project see E. Aprile *et al.*, Nucl. Phys. Proc. Suppl. **138**, 156 (2005) [arXiv:astro-ph/0407575]; For the SuperCDMS project see P. L. Brink *et al.* [CDMS-II Collaboration] [arXiv:astro-ph/0503583].

- [22] G. Belanger, F. Boudjema, A. Pukhov and A. Semenov, *Comput. Phys. Commun.* **176**, 367 (2007) [arXiv:hep-ph/0607059]; and arXiv:0803.2360 [hep-ph].
- [23] O. J. P. Eboli and D. Zeppenfeld, *Phys. Lett. B* **495**, 147 (2000) [arXiv:hep-ph/0009158].
- [24] D. Cavalli *et al.*, arXiv:hep-ph/0203056.
- [25] H. Davoudiasl, T. Han and H. E. Logan, *Phys. Rev. D* **71**, 115007 (2005) [arXiv:hep-ph/0412269];
- [26] S. h. Zhu, *Eur. Phys. J. C* **47**, 833 (2006) [arXiv:hep-ph/0512055].
- [27] R. M. Godbole, M. Guchait, K. Mazumdar, S. Moretti and D. P. Roy, *Phys. Lett. B* **571**, 184 (2003) [arXiv:hep-ph/0304137]; M. Heldmann, *Acta Phys. Polon. B* **38**, 787 (2007).
- [28] ATL-PHYS-PUB-2006-009; ATL-PHYS-PUB-2005-011;
- [29] M. Malawski, arXiv:hep-ph/0407160; B. P. Kersevan, M. Malawski and E. Richter-Was, *Eur. Phys. J. C* **29**, 541 (2003) [arXiv:hep-ph/0207014].
- [30] R. S. Hundi, B. Mukhopadhyaya and A. Nyffeler, *Phys. Lett. B* **649**, 280 (2007) [arXiv:hep-ph/0611116].
- [31] Q. H. Cao, E. Ma and G. Rajasekaran, *Phys. Rev. D* **76**, 095011 (2007) [arXiv:0708.2939 [hep-ph]].
- [32] G. Aad *et al.* [The ATLAS Collaboration], arXiv:0901.0512 [Unknown]; Kajari Mazumdar, CMS Collaboration, private communication.
- [33] A. Pukhov *et al.*, Preprint INP MSU 98-41/542; A. Pukhov *et al.*, arXiv:hep-ph/9908288; A. Pukhov, arXiv:hep-ph/0412191.
- [34] S. G. Frederiksen, N. Johnson, G. L. Kane and J. Reid, *Phys. Rev. D* **50**, 4244 (1994).